Desalination and Water Treatment
www.deswater.com

doi: 10.5004/dwt.2020.24958

184 (2020) 86–93
April

Experimental study on the structure of spacer in a flow-electrode capacitive deionization

Majid Nikfar[a], Ali Akbar Alemrajabi[a,*], KoYeon Choo[b], Youngjik Youn[b], Dong Kook Kim[b,*]

[a]*Department of Mechanical Engineering, Isfahan University of Technology, Isfahan, Iran, Tel.+98 31 33915207; Fax: +98 31 33912628; emails: rajabi@cc.iut.ac.ir (A.A. Alemrajabi), m.nikfar@me.iut.ac.ir (M. Nikfar)*
[b]*Separation and Conversion Materials Laboratory, Korea Institute of Energy Research, Daejeon, Republic of Korea, Tel. +82 42860 3133; Fax: +82 42 860 3152; emails: dokkim@kier.re.kr (D.K. Kim), kychoo@kier.re.kr (K.Y. Choo), youngjik2002@gmail.com (Y.J. Youn)*

Received 30 April 2018; Accepted 25 September 2019

ABSTRACT

The flow-electrode capacitive deionization (FCDI) technology has recently been actively studied as a means of easy scale-up for mass desalination based on the principle of an electric double-layer capacitor. In this study, we investigated the structural characteristics of a porous insulating spacer, which determines the desalting performance. The effect of parameters, such as thickness, porosity, wettability, and flow rates of saltwater (FR_w) have been investigated. As a result, for $FR_w \geq 2$ mL/min the desalting efficiency increases with decreasing the spacer's thickness, but for $FR_w < 2$ mL/min the optimum thickness was found to be 0.6 mm in terms of desalting efficiency. Utilizing a 0.3 mm thickness spacer lead to the best configuration in the FCDI setup based on the current efficiency criteria. The results show that the optimum porosity for the porous spacer was 0.56 in terms of desalting efficiency and salt removal rate while the spacer with 0.44 porosity has the best performance based on the current efficiency. In particular, wettability did not affect performance. It is observed that desalting efficiency increases as FR_w decreases.

Keywords: Water desalination; Capacitive deionization; Porous spacer; Thickness; Porosity; Wettability

1. Introduction

The water crisis in the world is an important problem that mankind has to face up. It is estimated that 3 billion people will live below the water stress threshold by 2025 [1]. Today, water desalting is not only a field of interest but also it is a necessary field for many researchers and their countries. There are different technics for water desalination such as; multi-stage flash [2,3], multiple-effect distillation [4], mechanical vapor compression [5,6], freezing [7], humidification–dehumidification [8], solar still [9–11], reverse osmosis [12], electrodialysis [13], and capacitive deionization (CDI) or capacitive desalination [14–16].

CDI is an electrochemical water treatment technology based on the formation of an electrical double layer on the surface of porous electrode materials under an electrical field. The basic type of this system consists of two carbon porous electrodes which are fixed on both sides of a channel so that electrolyte flows between the electrodes. The ions are adsorbed to the opposite electrodes by applying an electrical potential on the electrodes. It must be noted that carbon functionality plays a significant role in CDI [17,18].

* Corresponding authors.

Among water desalination technics, capacitive desalination has been increasingly studied. A study on this system is of interest due to its advantages such as smaller footprint, fairly low energy usage [14,15,19], and low cost, because the direct electrosorption of ions in saltwater on porous electrodes needs a low operating voltage of about 1.2 V.

In recent years, many experimental studies have been done, some sub-models for adsorption of ions are suggested, and several researchers have investigated CDI from various perspectives [20–29]. Among these researches, there are some studies on new types of cell geometry, such as flow-through CDI [30], wire-based CDI [31], and flow-electrode CDI [32–35].

In flow-electrode capacitive deionization (FCDI), slurry activated carbon (AC) replaces fixed electrode in a conventional CDI. The suspended AC adsorbs the ions when an external electric potential is applied to the current collector. The adsorbed ions are carried by the flow of electrodes. The cation and anion exchange membranes just allow one special ion to pass, positive or negative, respectively. So, the FCDI cell generally separates the ions in the feed water [32].

In the previous works, FCDI is introduced [32] and some aspects of it were investigated [36–40]. FCDI has some advantages over CDI. The important advantage is that FCDI is a continuous system and the discharge step is not needed as compared to the general CDI. Easy scaling up is another advantage of FCDI [39,40].

The FCDI cell consists of four key parts, that is, a current collector carved with a microchannel, a slurry electrode, ion exchange membranes, and a spacer. In an FCDI system, the current collector is very important because the flowability of slurry electrodes affects FCDI performance. Also, structural characteristics of the porous spacer is an important factor because of its effect on the desalting efficiency and flowability of saltwater. Especially, porous spacer has two functions, that is, insulation of cathode/anode, and preparing a channel for continuous flow of saltwater. In the present study, the effects of thickness and porosity of the porous spacer in an FCDI cell are investigated for different flow rates of saltwater.

2. Experimental setup

2.1. FCDI set

Figs. 1a–c shows an FCDI cell. The FCDI is composed of a pair of graphite current collectors, cation- or anion-exchange

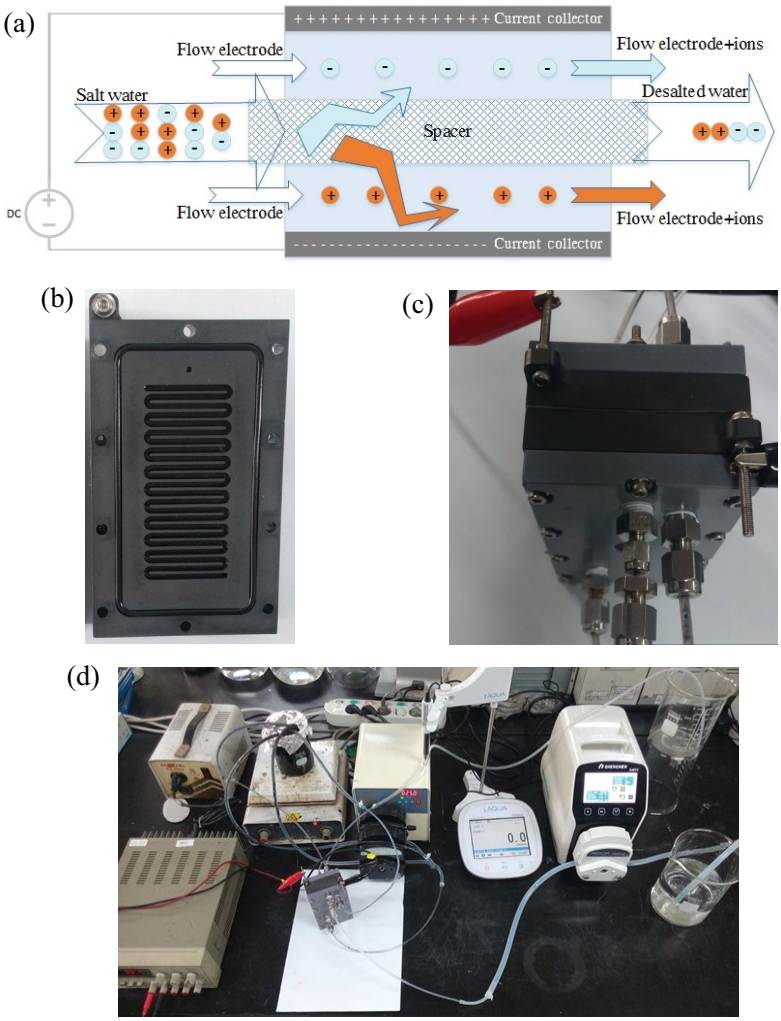

Fig. 1. (a) Scheme photo of an FCDI cell, (b) current collector with carved flow electrode channel, (c) FCDI cell, and (d) FCDI setup.

membranes, a gasket, a spacer, and one pair of endplates. The width, length, and height of the graphite current collectors are 110, 66, and 12 mm, respectively. The carved flow channel on the collectors is 2 mm in width and 2 mm in depth. The column length of each 23 flow channels is 30 mm. The thickness of the ion-exchange membranes was around 160 μm (Neosepta CMX and AMX, Tokuyama, Japan). The contact area between the ion-exchange membranes and flow-electrode was 12.7 cm^2. A silicone gasket and a 0.3 mm thick polyester spacer were utilized between cation and anion-exchange membranes for assembling the FCDI unit cell. All parts were held together using polyvinyl chloride endplates.

2.2. Operation of FCDI unit cell

Fig. 1d shows the setup of the FCDI unit cell. The salt concentration in the NaCl solution is 35 g/L. The saltwater flows through the spacer at several flow rates from 0.5 to 10 mL/min between the ion-exchange membranes. The saltwater is operated under open-cycle conditions with two reservoirs (saltwater and desalinated water reservoirs). The flow rate of the flow-electrode, operated in a closed cycle, was maintained constant at 21.5 mL/min. The flow-electrode ran along the flow path on the current collector. The fresh cathode and anode flow-electrode come out from one flow-electrode reservoir to the FCDI unit cell. As shown in Fig. 1, the used cathode and anode flow-electrodes are accumulated into the one flow-electrode reservoir. As shown in the previous study [36], this operation method originated from the automatic release of ions electrostatically adsorbed on the surface of AC after desalting by mixing and neutralizing the charged cathode and anode flow-electrodes. Consequently, the desalting performance of flow-electrodes was restored by the simple mixing of the charged cathode and anode flow-electrodes [37].

Each desalting experiment was performed for 30 min. A pre-determined time interval between the two consecutive experiments is introduced for attaining the initial electrical conductivity of the effluent after the release of voltage. After conducting the desalting experiments three times, another experiment is done. A constant voltage of 1.2 V was applied to the FCDI unit cell using a power supply (E3630A, triple output direct current power supply, HEWLETT PACKARD, Republic of Korea) for desalting experiments. The salt concentration in the output of saltwater was obtained from its measured electrical conductivity, using a conductivity meter (F-74, LAQUA, HORIBA Scientific, Japan). Before the experiments, all measuring devices were calibrated.

2.3. Physical properties of AC flow-electrode

The flow-electrode, which comprised a slurry AC, was made from a homogeneous dispersion of commercial AC (Maxsorb MSC-30, Kansai Coke and Chemicals Co. Ltd., Japan) in a 0.1 M aqueous solution of NaCl. The weight ratio of deionized water to spherical AC was 10:1. The mixtures were stirred using a magnetic bar for 24 h for achieving a homogeneous carbon suspension [38].

The shape of spherical AC was verified by field emission scanning electron microscopy (FESEM, JSM-6700F, JEOL Ltd., Japan). The average size of the spherical AC particles was 12.83 μm at D_{50}. The specific surface area, average pore diameter, and total pore volume of the spherical AC particles were 3,011 m^2/g, 2.49 nm, and 1.63 cm^3/g, respectively [38].

3. Results and discussions

As said before, in this study effects of thickness, porosity, and wettability of the spacer on desalting performance are investigated for several volume flow rates of saltwater (FR_w). In this study; the thickness of a single spacer is 0.3 mm and the spacer is made of polyester. The concentration of inlet saltwater (C_{in}) is 35 g/L, which is, the same as seawater. Also, the volume flow rate of the electrode (FR_e) is kept constant at 21.5 mL/min.

To evaluate the desalting performance of FCDI, few parameters are used. The desalting efficiency is defined as:

$$E(\%) = \frac{C_{in} - C_{out}}{C_{in}} \times 100 \quad (1)$$

where C_{in} is the inlet concentration of the influent (g/L), C_{out} is the minimum concentration of the effluent (g/L), respectively. The salt removal rate (R) was introduced in a previous study [32] as the following:

$$R = \frac{Q_f \times (C_{in} - C_{out})}{A} \quad (2)$$

where Q_f is the volumetric flow rate (L/min) and A is the contact area (cm^2). Another important parameter is the current efficiency [34,38] defines as:

$$\eta(\%) = \frac{Q_f \times F \times (C_{in} - C_{out})}{M \times I} \times 100 \quad (3)$$

where η is the current efficiency, the ratio of desalting flux over current density I (divided by Faraday's number (F), F = 96,485 C/mol), Q_f is the volume flow rate of the influent (L/s), M is the molar mass of NaCl which is 58 g/mol, the chemical valiancy of NaCl is 1, and I is the current at the point of minimum concentration of the effluent (A).

Each experiment was repeated a few times and the average results are presented here.

Firstly, the effect of the wettability of the spacer is investigated. In this regard, two types of spacer with similar thickness and porosity, but of different wettability, that is, high and low wettability, are tested. In this regard, the contact angle is measured (by SEO contact angle analyzer (PHOENIX 450, Korea)) for 5 s in 1 s increments after the water droplet touched the sample surface. Figs. 2a and b show these 2 spacers with different contact angles. It can be seen that the contact angle for spacer (a), after 5 s, is near zero, which means high wettability. Oppositely, spacer (b) has a contact angle lower than 90°, so it has low wettability. Fig. 3 shows desalting efficiency (E) for high and low wettability of spacer for 4 flow rates (FR_w) of 2, 2.5, 3, and 5 mL/min. Results show that the effect of wettability of spacer on the desalting efficiency is insignificant. It seems that the attraction force of ions to the electrodes is much higher than the attraction force

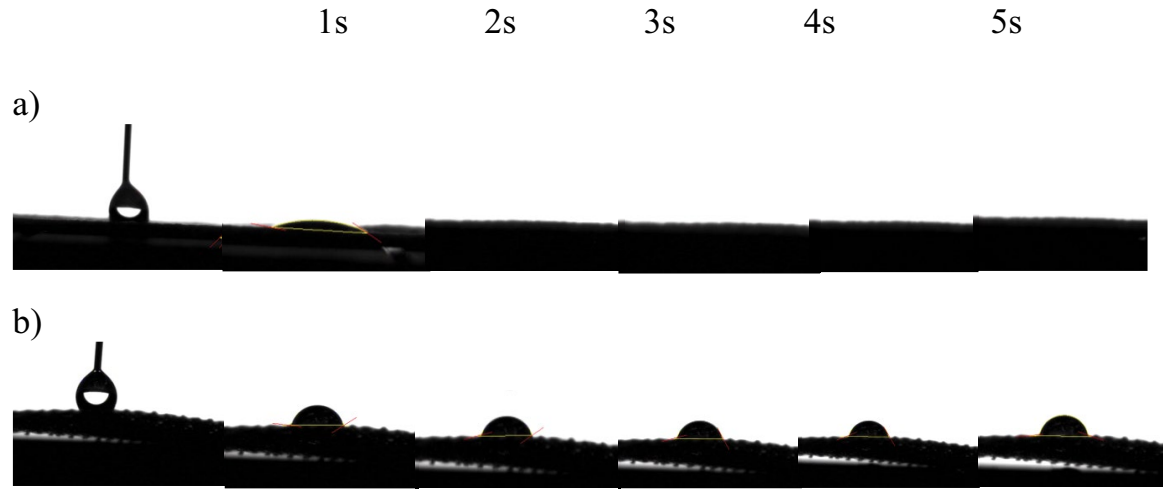

Fig. 2. Contact angle of the 2 kinds of spacer (a) high wettability and (b) low wettability.

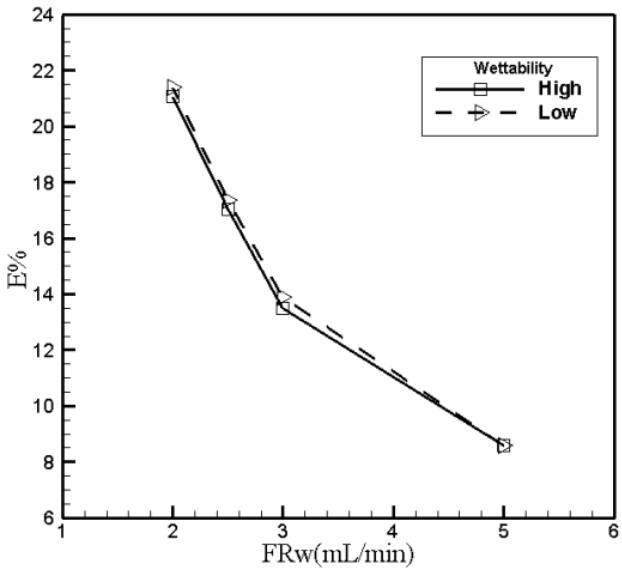

Fig. 3. Desalting efficiency, E(%) of spacers vs. wettability for different flow rates.

between the spacer and water drops. Therefore, the effect of wettability on desalting efficiency is very low.

To investigate the effect of thickness of the spacer on desalting efficiency, four different thicknesses were examined. Each spacer has a thickness of 0.3 mm. therefore, to apply different thicknesses; one to four layers of spacer were used. In this part, the volume flow rate of saltwater, FR_w, is varied from 0.5 to 10 mL/min.

Fig. 4a shows the results of the effect of spacer thickness and volume flow rate of saltwater on desalting efficiency, E(%). The porosity of the spacer is 0.44. Two counter effects of the spacer thickness are noticeable. As the spacer thickness increases, the cross-sectional area of flow increases which results in lower velocity and higher contact time between saltwater and electrodes which tends to increase desalting efficiency. On the other hand, an increase in spacer thickness makes the electrodes more apart which tends to reduce the desalting efficiency. It must be noted that the contact surface area is the same for all spacer thicknesses. From Fig. 4 it can be seen that, generally, the desalting efficiency increases with decreasing the spacer's thickness with the exception that for $FR_w < 2$ mL/min the desalting efficiency is higher by 18% at a thickness of 0.6 mm as compared to the thickness of 0.3 mm. On the other hand, it can be seen that at the high flow rates, the desalting efficiency is insensitive to the spacer thickness.

Fig. 4b shows the salt removal rate (R) vs. flow rate of saltwater for different thicknesses of the spacer. According to the results, the salt removal rate is the lowest at the lowest flow rates, regardless of the spacer thickness. This is in contrast to the desalting efficiency as shown in Fig. 4a. At first, R increases by increasing FR_w up to $FR_w = 2$ mL/min. After that, the increase in FR_w leads to the oscillating behavior of R.

An increase in the retention time of saltwater in the cell leads to an increase in desalting parameter ($C_{in} - C_{out}$) and desalting efficiency. On the other hand spending time of desalting (taking longer time associated with a decrease in flow rate), has a negative effect on the salt removal rate. The maximum and minimum R curve vs. FR_w is due to the confrontation between the two mentioned factors.

Fig. 4c shows the current efficiency η vs. flow rate of saltwater for different thicknesses of the spacer. Results show the current efficiency is maximum at the lowest flow rate, FR_w = 0.5 mL/min (opposite to salt removal rate, Fig. 4b) regardless of the spacer thickness. In general, (especially at the middle range of FR_w), the thinnest spacer (with 0.3 mm thickness) has the best current efficiency. In other words, the 0.3 mm thickness spacer makes the best configuration for this FCDI setup upon current efficiency.

Considering that at higher flow rates, the consumption of energy increases (especially in the pumps), the removal efficiency decreases, and wear and tear of the equipment increases, the flow rates of 1–3 mL/min are recommended for salt removal.

The effect of spacer porosity on the desalting efficiency at a constant spacer thickness of 0.3 mm for different flow

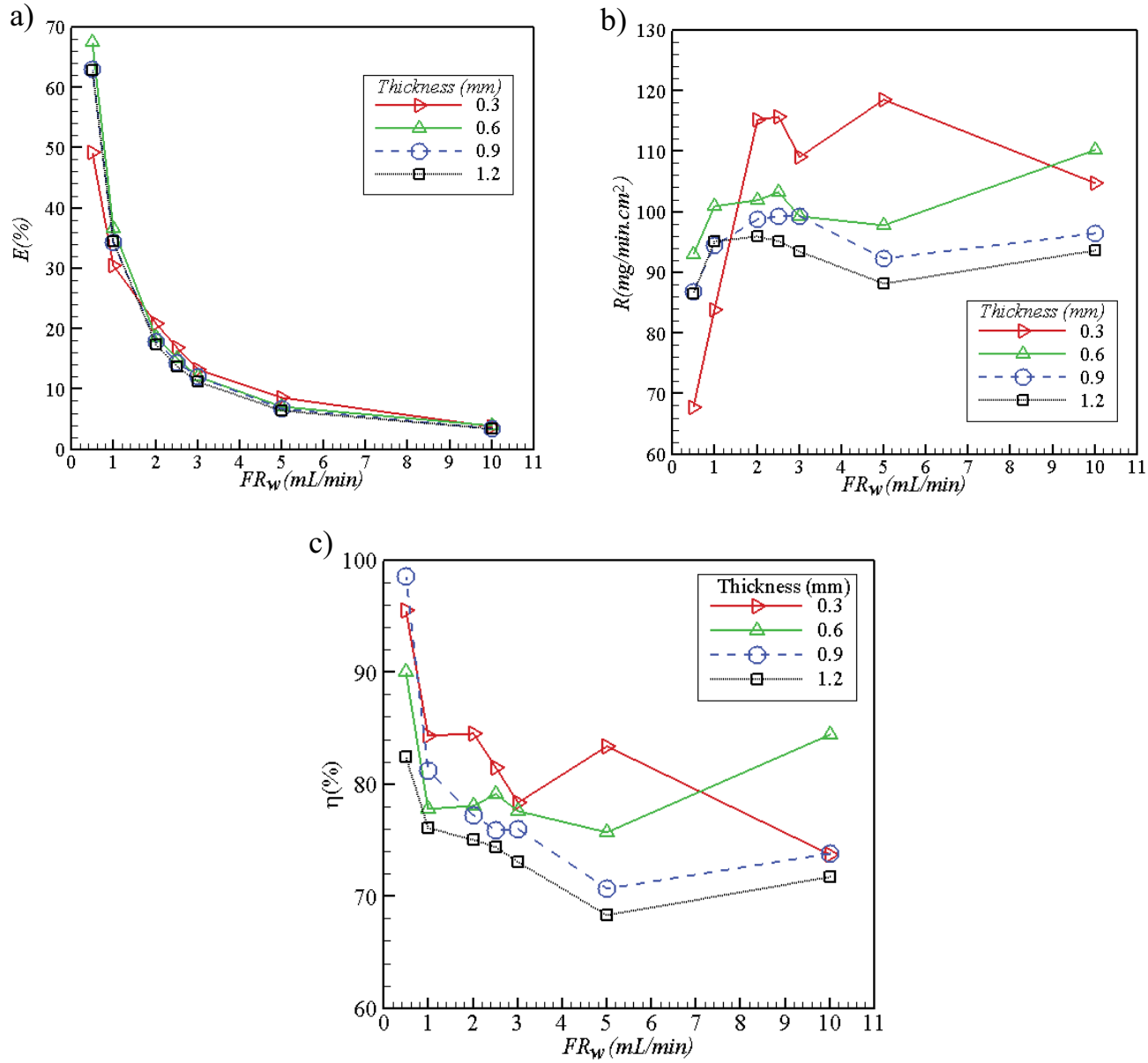

Fig. 4. Effect of thickness and volume flow rate of saltwater (FR_w) on the (a) desalting efficiency (E(%)), (b) salt removal rate (R), and (c) current efficiency (η(%)).

rates and velocities was studied and the results are depicted in Fig. 5. The velocity can be derived from the flow rate by considering the porosity of spacer (ε) and cross-section area of saltwater flow (the thickness-oriented section area, Ac = 9.45 mm²):

$$V = \frac{FR_w}{Ac \times \varepsilon} \quad (4)$$

Figs. 5a and b show the desalting efficiency for different porosities, based on different flow rates and velocity, respectively. From Fig. 5a it can be observed that the spacer porosity of 0.56 has the best desalting efficiency among the porosities studied (at a constant flow rate of saltwater). From Fig. 5a the second-best spacer porosity was 0.44. In other words, at a constant FR_w, the higher and lower porosities have lower desalting efficiencies than the two-mentioned porosities. At low porosities, pore areas are small and the flow velocity throughout the pores, increases (at a constant flow rate) which in turn leads to lower efficiency (Fig. 5a). This means that for a constant porosity of the spacer, the desalting efficiency decreases by an increase in the velocity of saltwater (Fig. 5b). It can be seen that within a given range of the velocity the spacer with the lowest porosity has the best desalting efficiency. For example in the domain of 7–9 L/(min m²) the spacer with a porosity of 0.36 has the highest desalting efficiency.

On the other hand, at high porosities which is accompanied by high pore area, lower pressure drop and the tortuosity of porous media decreases [41] which in turn leads to

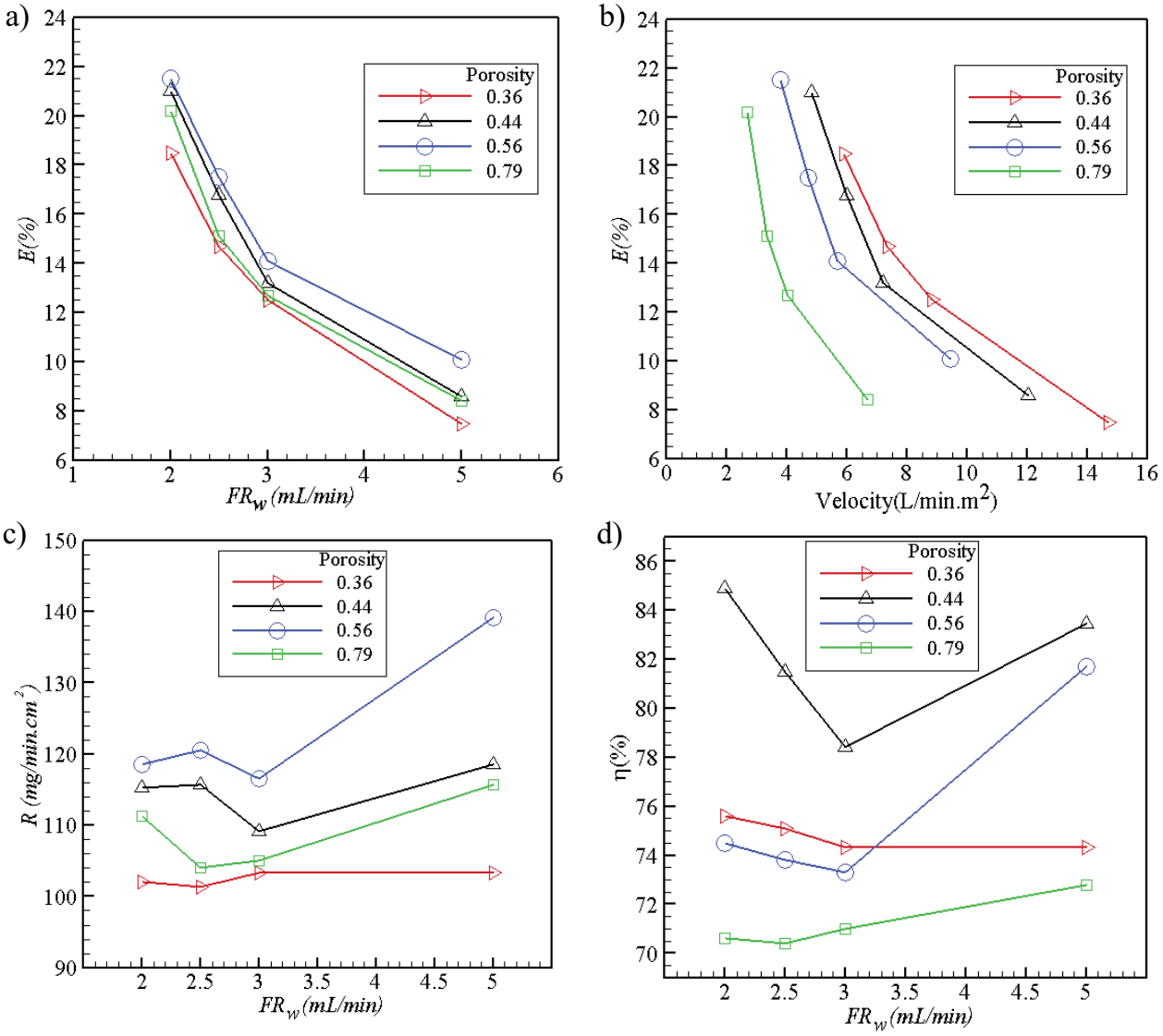

Fig. 5. Performance of the set vs. porosity (a) desalting efficiency per-flow rates (FR_w), (b) desalting efficiency per velocity, (c) salt removal rate (R), and (d) current efficiency (η(%)).

less mixing of flow and lower salt gradient at the vicinity of electrodes, hence lower desalting efficiency (Figs. 5a and b).

Fig. 5c shows the salt removal rate (R) vs. flow rate of saltwater for different porosity of the spacer. According to the results, the salt removal rate is the maximum at FR_w = 5 mL/min, regardless of the porosity. From Fig. 5c it can be observed that the spacer porosity of 0.56 has the best salt removal rate among the porosities studied for all flow rates of saltwater. Fig. 4d shows the current efficiency η vs. flow rate of saltwater for different porosity of the spacer. Results show that the spacer with porosity of 0.44 has the best performance based on current efficiency. It means that in this FCDI set, the spacer with 0.44 porosity is matched with other parts so that their assembly results in the highest η. More data is needed to correlate the optimum thickness and porosity in any setup.

In response to the question that what would the batch performance of such assembly be, 200 mL saltwater with C_{in} = 35 gr/L (seawater) was circulated in a closed-loop for 20 h, and the parameters were considered at the end of this period. In this test, FR_w and FR_e are 2.5 and 21.5 mL/min, respectively. The thickness of the spacer was 0.3 mm and its porosity was 0.44.

Results show that at the end of this period, the desalting was sufficient to produce drinkable water with 1 g/L NaCl. The desalting efficiency was about 97%. The desalination time decreases by increasing the contact surface of saltwater and flow electrodes, as big as the size FCDI or Stack design of FCDI [32,39]. This test proves that FCDI cells can decrease the salt concentration of seawater to potable levels.

4. Conclusions

The effects of thickness, porosity, and wettability of the porous spacer in an FCDI set are experimentally investigated. The tests are done for several flow rates of saltwater (FR_w).

Four thicknesses, that is, 0.3, 0.6, 0.9, and 1.2 mm are used. Results show that while for $FR_w \geq 2$ mL/min, the desalting efficiency increases with decreasing the spacer's thickness and the 0.3 mm spacer has higher efficiency, for $FR_w < 2$ mL/min the best desalting efficiency corresponds to the 0.6 mm thickness. According to the results, for the spacer with 0.44 porosity, the salt removal rate and current efficiency are the lowest and highest, respectively, at the lowest flow rate (regardless of the spacer thickness). This behavior may vary for different porosities. Considering that at higher flow rates, the consumption of energy increases, the removal efficiency decreases, and wear and tear of the equipment increases, the flow rates of 1–3 mL/min are recommended for salt removal. Generally, utilizing the 0.3 mm thickness spacer leads to the best configuration for this FCDI setup upon current efficiency criteria. The results also show that the porous spacer with porosity of 0.56 has the best desalting efficiency and salt removal rate among the porosities studied (at a constant FR_w) while the spacer with 0.44 porosity has the best performance based on current efficiency. On the other hand, for a constant porosity of the spacer, the desalting efficiency decreases by increasing of velocity of saltwater, while the spacer with the lowest porosity (0.36) has the best desalting efficiency at a constant velocity of saltwater. More data is needed to correlate the optimum thickness and porosity in any setup.

Results show that the wettability of the spacer has not a significant effect on the desalting efficiency. Generally, desalting efficiency is increased by decreasing of FR_w. The set up was capable of desalting salty water of sea level salt concentration to a potable level with a desalting efficiency of 97%.

Acknowledgments

This research was supported by Isfahan University of Technology (IUT). Also the research was supported by the Technology Development Program to Solve Climate Changes of the National Research Foundation (NRF) funded by the Ministry of Science and ICT (2017M1A2A2047366).

References

[1] https://www.treehugger.com/clean-water/water-shortages-rising-across-the-globe-but-especially-india.html, Report, Last Seen Jan. 2018.
[2] M.A. Darwish, N.M. Al-Najem, Energy consumption by multi-stage flash and reverse osmosis desalters, Appl. Therm. Eng., 20 (2000) 399–416.
[3] H. El-Dessouky, H. Ettouney, H. Al-Fulaij, F. Mandani, Multistage flash desalination combined with thermal vapor compression, Chem. Eng. Process., 39 (2000) 343–356.
[4] M. Al-Shammiri, M. Safar, Multi-effect distillation plants: state of the art, Desalination, 126 (1999) 45–59.
[5] H. Ettouney, Visual basic computer package for thermal and membrane desalination processes, Desalination, 165 (2004) 393–408.
[6] F. Mandani, H. Ettouney, H. El-Dessouky, LiBr-H_2O absorption heat pump for single-effect evaporation desalination process, Desalination, 128 (2000) 161–176.
[7] M.W. Tleimat, Freezing Methods. Principles of Desalination, Part B, 2nd ed., K.S. Spiegler, A.D. Laird, Eds., Academia Press, New York, 1980, pp. 360–400.
[9] J. Lindblom, Solar Thermal Technologies for Seawater Desalination: State of the Art, in Solar Energy, Danmarks Tekniske Universitet, Lyngby, 2003, pp. 93–108.
[10] R. Bhardwaj, M.V. ten Kortenaar, R.F. Mudde, Maximized production of water by increasing area of condensation surface for solar distillation, Appl. Energy, 154 (2015) 480–490.
[11] S. Gorgian, Development and Evaluation of a Point-Focus Parabolic Solar Still, Ph.D. Thesis, Tarbiat Modares University Faculty of Agriculture, Iran, 2013.
[12] B. Van der Bruggen, Desalination by distillation and by reverse osmosis — trends towards the future, Membr. Technol., 2 (2003) 6–9.
[13] Y. Gong, X.-l. Wang, L.-x. Yu, Process simulation of desalination by electrodialysis of an aqueous solution containing a neutral solute, Desalination, 172 (2005) 157–172.
[14] M.E. Suss, S. Porada, X. Sun, P.M. Biesheuvel, J. Yoon, V. Presser, Water desalination *via* capacitive deionization: what is it and what can we expect from it?, Energy Environ. Sci., 8 (2015) 2296.
[15] S. Porada, R. Zhao, A. van der Wal, V. Presser, P.M. Biesheuvel, Review on the science and technology of water desalination by capacitive deionization, Prog. Mater Sci., 58 (2013) 1388–1442.
[16] K. Laxman, Water Desalination by Nanostructuring Enhanced Control of Capacitive Deionization, Ph.D. Thesis, Department of Electrical and Computer Engineering College of Engineering, Sultan Qaboos University, Sultanate of Oman, 2015.
[17] X. Gao, A. Omosebi, J. Landon, K.L. Liu, Surface charge enhanced carbon electrodes for stable and efficient capacitive deionization using inverted adsorption–desorption behavior, Energy Environ. Sci., 8 (2015) 897–909.
[18] X. Gao, S. Porada, A. Omosebi, K.-L. Liu, P.M. Biesheuvel, J. Landon, Complementary surface charge for enhanced capacitive deionization, Water Res., 92 (2016) 1–8.
[19] A. Subramani, M. Badruzzaman, J. Oppenheimer, J.G. Jacangelo, Energy minimization strategies and renewable energy utilization for desalination: a review, Water Res., 45 (2011) 1907–1920.
[20] K. Laxman, L. Al Gharibi, J. Dutta, Capacitive deionization with asymmetric electrodes: electrode capacitance vs electrode surface area, Electrochim. Acta, 176 (2015) 420–425.
[21] L. Zou, G. Morris, D. Qi, Using activated carbon electrode in electrosorptive deionisation of brackish water, Desalination, 225 (2008) 329–340.
[22] P. Xu, J.E. Drewes, D. Heil, G. Wang, Treatment of brackish produced water using carbon aerogel-based capacitive deionization technology, Water Res., 42 (2008) 2605–2617.
[23] S. Porada, L. Weinstein, R. Dash, A. van der Wal, M. Bryjak, Y. Gogotsi, P.M. Biesheuvel, Water desalination using capacitive deionization with microporous carbon electrodes, ACS Appl. Mater. Interfaces, 4 (2012) 1194–1199.
[24] C. Tsouris, R. Mayes, J. Kiggans, K. Sharma, S. Yiacoumi, D. DePaoli, S. Dai, Mesoporous carbon for capacitive deionization of saline water, Environ. Sci. Technol., 45 (2011) 10243–10249.
[25] L. Wang, M. Wang, Z.-H. Huang, T.X. Cui, X.C. Gui, F.Y. Kang, K.L. Wang, D.H. Wu, Capacitive deionization of NaCl solutions using carbon nanotube sponge electrodes, J. Mater. Chem., 21 (2011) 18295–18299.
[26] H. Wang, D.S. Zhang, T.T. Yan, X.R. Wen, L.Y. Shi, J.P. Zhang, Graphene prepared via a novel pyridine–thermal strategy for capacitive deionization, J. Mater. Chem., 22 (2012) 23745–23748.
[27] N.-S. Kwak, J.S. Koo, T.S. Hwang, E.M. Choi, Synthesis and electrical properties of NaSS–MAA–MMA cation exchange membranes for membrane capacitive deionization (MCDI), Desalination, 285 (2012) 138–146.
[28] Y.W. Choi, M.S. Lee, T.H. Yang, Y.G. Yoon, S.H. Park, D.K. Kim, S.C. Yang, Ion Exchange Membrane for Flow-Electrode Capacitive Deionization Device and Flow-Electrode Capacitive Deionization Device Including the Same, Patent, EP 2857442, 2015.
[29] R. Zhao, P.M. Biesheuvel, A. van der Wal, Energy consumption and constant current operation in membrane capacitive deionization, Energy Environ. Sci., 5 (2012) 9520–9527.
[30] M.E. Suss, T.F. Baumann, W.L. Bourcier, C.M. Spadaccini, K.A. Rose, J.G. Santiago, M. Stadermann, Capacitive desalination with flow-through electrodes, Energy Environ. Sci., 5 (2012) 9511–9519.

[31] S. Porada, B.B. Sales, H.V.M. Hamelers, P.M. Biesheuvel, Water desalination with wires, J. Phys. Chem. Lett., 3 (2012) 1613–1618.
[32] S.-i. Jeon, H.-r. Park, J.-g. Yeo, S.C. Yang, C.H. Cho, M.H. Han, D.K. Kim, Desalination *via* a new membrane capacitive deionization process utilizing flow-electrodes, Energy Environ. Sci., 6 (2013) 1471–1475.
[33] K.B. Hatzell, E. Iwama, A. Ferris, B. Daffos, K. Urita, T. Tzedakis, F. Chauvet, P.-L. Taberna, Y. Gogotsi, P. Simon, Capacitive deionization concept based on suspension electrodes without ion exchange membranes, Electrochem. Commun., 43 (2014) 18–21.
[34] S. Porada, D. Weingarth, H.V.M. Hamelers, M. Bryjak, V. Presser, P.M. Biesheuvel, Carbon flow electrodes for continuous operation of capacitive deionization and capacitive mixing energy generation, J. Mater. Chem. A, 2 (2014) 9313–9321.
[35] A. Rommerskirchen, Y. Gendel, M. Wessling, Single module flow-electrode capacitive deionization for continuous water desalination, Electrochem. Commun., 60 (2015) 34–37.
[36] S.-i. Jeon, J.-g. Yeo, S.C. Yang, J.Y. Choi, D.K. Kim, Ion storage and energy recovery of a flow-electrode capacitive deionization process, J. Mater. Chem. A, 2 (2014) 6378–6383.
[37] S.C. Yang, J.Y. Choi, J.-g. Yeo, S.-i. Jeon, H.-r. Park, D.K. Kim, Flow-electrode capacitive deionization using an aqueous electrolyte with a high salt concentration, Environ. Sci. Technol., 50 (2016) 5892–5899.
[38] H.-r. Park, J.Y. Choi, S.C. Yang, S.J. Kwak, S.-i. Jeon, M.H. Han, D.K. Kim, Surface-modified spherical activated carbon for high carbon loading and its desalting performance in flow-electrode capacitive deionization, R. Soc. Chem., 6 (2016) 69720–69727.
[39] S.C. Yang, S.-i. Jeon, H. Kim, J. Choi, J.-g. Yeo, H.-r. Park, D.K. Kim, Stack design and operation for scaling up the capacity of flow-electrode capacitive deionization technology, ACS Sustainable Chem. Eng., 4 (2016) 4174–4180.
[40] Y.Y. Cho, K.S. Lee, S.C. Yang, J. Choi, H.-r. Park, D.K. Kim, A novel three-dimensional desalination system utilizing honeycomb-shaped lattice structures for flow-electrode capacitive deionization, Energy Environ. Sci., 10 (2017) 1746–1750.
[41] K. Vafai, Handbook of Porous Media, 3rd ed., CRC Press Taylor & Francis Group, Boca Raton, Florida, 2015.